Probing Conformation Change and Binding Mode of Metal Ion-Carboxyl Coordination Complex through Resonant Surface-Enhanced Raman Spectroscopy and Density Functional Theory

Willis Kwun Hei Ho,[†,#] Zhi Yong Bao,[†,‖,#] Xiaorong Gan,[‡,Ω,#] Kwok-Yin Wong,[,‡] Jiyan Dai,*[,†] Dangyuan Lei*[,†,§]*

† Department of Applied Physics, The Hong Kong Polytechnic University, Hong Kong, China

‡ Department of Applied Biology and Chemical Technology, The Hong Kong Polytechnic University, Hong Kong, China

§ Department of Materials Science and Engineering, City University of Hong Kong, Hong Kong, China

‖ School of Materials Science and Engineering, Hefei University of Technology, Hefei, China

Ω College of Environment, HoHai University, Nanjing, China

AUTHOR INFORMATION

Corresponding Authors

*kwok-yin.wong@polyu.edu.hk; jiyan.dai@polyu.edu.hk; dangylei@cityu.edu.hk.

Abstract

Understanding of carboxyl-metal ligand interaction has great significance in analytical chemistry. Herein, we use resonant surface-enhanced Raman scattering (SERS) to probe the physiochemical interaction and conformation change in several metal ion-carboxyl coordination complex systems adsorbed on plasmonically resonant metal nanostructures surface. Our SERS results and density function theory calculations jointly reveal that low-valence metal ions (such as K^+ and Pb^{2+}) tend

to bind to the carboxyl active site of a Raman tag molecule, 4-mercaptobenzoic acid (4-MBA), in a unidentate binding mode of low binding energy whereas high-valence metal ions (such as Fe^{3+}) favor a bidentate binding mode of relatively high binding energy. Particularly, Pb^{2+} ion concentration-dependent SERS spectra suggest the repulsive interaction leads to a tilted configuration of 4-MBA on the metal surface. This work indicates the resonant SERS approach not only suits for studying carboxyl-metal ligand interaction but also detecting various types of heavy metal ions at low concentrations.

TOC GRAPHICS

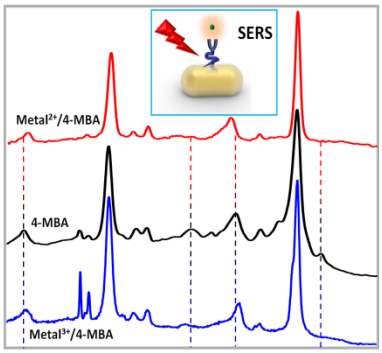

KEYWORDS resonant surface-enhanced Raman spectroscopy, density function theory, carboxyl-metal-ion ligand interaction, surface plasmon resonance, molecular conformation

Ligand interaction between metal ions and functional groups plays a crucial role in biochemistry and life science. For example, metalloproteins such as hemoglobin and DNA/RNA polymerase are mediated by metal ion cofactors, and as a result oxygen transportation[1-2] and DNA/RNA synthesis[3-4] can be precisely controlled. It is also reported that Mg^{2+} ion can regulate the energy releasing process owning to its high binding affinity towards energy carrier adenosine triphosphate (ATP)[5-6]. Besides from the biotic systems, manipulating ligand-metal interaction is also essential

to artificially synthesized catalysts[7-9] and polymers[10-11]. Therefore, comprehensive understanding of the ligand complex interaction can provide constructive information to the aforementioned research fields.

X-ray[12-15], neutron diffraction[16-18] and nuclear magnetic resonance (NMR) are commonly employed to study the ligand complex interaction. However, these characterization techniques often require highly-concentrated samples, and also involve complicated sample preparation. To overcome these limitations, vibrational spectroscopies, which extract optical signals from the light-sample interaction, have emerged with easy implementation. For example, Raman scattering and Fourier-transform infrared spectroscopies have been employed to detect molecular conformational changes induced by metal-ligand interaction[19-22]. However, the optical signals derived from molecule-metal ion bond vibrations are often very weak, limiting the signal collection when the molecule concentration is relatively low[23]. To solve this problem associated with the intrinsically low Raman scattering cross-section of molecules, surface-enhanced Raman scattering (SERS) has been developed by utilizing the localized surface plasmon resonance (LSPR) in metallic nanostructures. Upon the excitation of LSPR, the incident light energy is absorbed and confined around the surface of a metallic nanostructure, which consequently produces strongly enhanced electromagnetic near fields[24-25] and thereby accelerates molecular vibrations, allowing an accurate and sensitive probing of molecular conformation changes.

Here, we combine resonant SERS spectroscopy and density functional theory (DFT) calculations to systematically study the physiochemical interaction and conformational change in several metal ion-carboxyl coordination complex. 4-mercaptobenzoic (4-MBA) molecule monolayer as a SERS tag of metal ions was assembled on an array of densely-packed gold nanorods (GNRs). Under resonant illumination at the localized surface plasmon resonance (LSPR) band of the GNRs, the

pure 4-MBA/GNR system exhibits several characteristic vibrational modes of 4-MBA. Upon the addition of metal ions, some of these Raman modes either red shift or blue shift, depending on the valence of the ions, and the amount of Raman shift is correlated with ion concentration and the pH value of the solution, thereby allowing a systematic spectral analysis on the metal ion-carboxyl ligand interaction in aqueous environment. The Pb^{2+} ion concentration-dependent SERS spectral analysis also suggests that 4-MBA adopts a tilted configuration at high concentrations of Pb^{2+}. Our experimental observations are well supported by the DFT calculations.

The resonant SERS nanostructure was made by assembling CTAB-capped GNRs on a glass substrate, assisted by electrostatic interaction. The left panel of Figure 1(a) shows a transparent bare glass slide and a greenish GNR-assembled slide. As seen from the scanning electron microscope (SEM) micrograph in the right panel, GNRs are uniformly dispersed on the glass slide with an estimated particle density of 110-120 GNRs/μm^2. UV-Vis spectroscopic measurements show that the absorption spectrum of the SERS substrate closely resembles that for an aqueous solution of the same GNRs, with the longitudinal LSPR peak shifting from 687 to 642 nm due to the decreased effective dielectric perimittivity[26-27]. The SERS substrate absorption peak exhibits no significant broadening, indicating that the GNR deposition has no aggregation, consistent with the SEM micrograph. The plasmonic response of individual GNRs is well persevered in this solid SERS substrate, providing a strong near-field enhancement under resonant excitation.

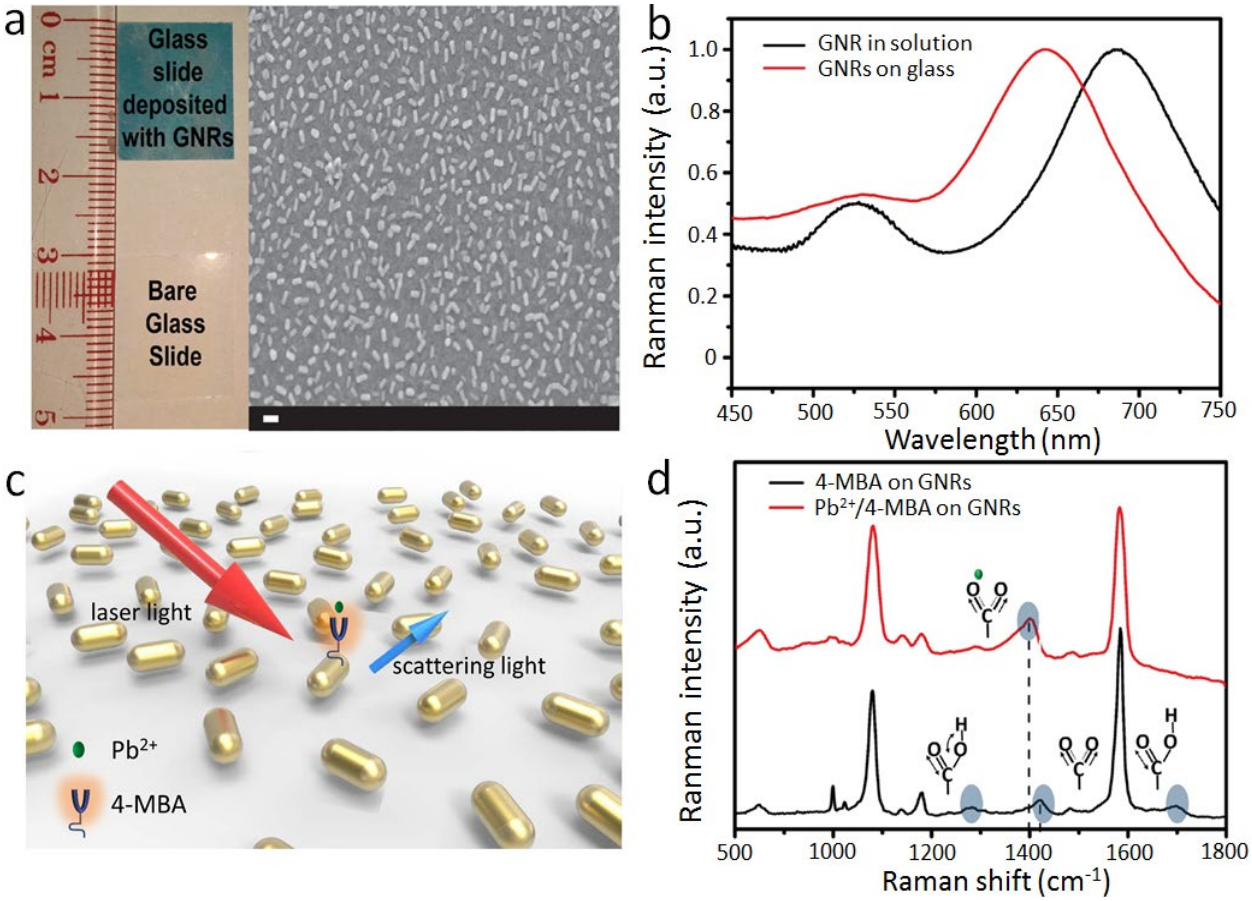

Figure 1. (a) Left: Photographs of a glass slide covered with dense GNRs (upper, greenish) and a bare glass slide (lower, transparent); Right: SEM micrograph of the GNG-covered glass slide, i.e. our solid SERS substrate. The white scale bar is 50 nm. (b) Normalized absorption spectra of the SERS substrate (red) and the same GNRs in water (black). (c) Schematic diagram of probing carboxyl-Pb^{2+} binding configuration with SERS. (d) SERS spectra of 4-MBA (black) and Pb^{2+}/4-MBA complex (red) both adsorbed on the surface of GNRs.

Here, 4-MBA is used as a Raman tag molecule because it can be tightly adsorbed on the surface of GNRs through forming Au-S bonding, and its functional carboxyl group has a strong binding affinity towards metal ions, which results in the formation of carboxyl-metal ion coordination complex. To investigate the physiochemical interaction in such coordination complex system, determine the mode of metal ion-carboxyl bonding, and also monitor molecular conformational change, as schematically illustrated in Figure 1(c), we collect the SERS signals of the system under

resonant excitation by a 633 nm CW laser, which closely matches the longitudinal LSPR wavelength of the GNRs. To confirm resonant excitation enhanced SERS, we compare the SERS signals collected from the same system under on-resonance excitation at 633 nm and off-resonance excitation at 488 nm at the same conditions, with the results shown in Figure S1. Indeed, the resonant excitation gives rise to an SERS intensity more than one order of magnitude larger than that of the non-resonant excitation.

We start with Pb^{2+} as a representative because monitoring Pb^{2+} at the trace level is of high importance to the public hygienic issue[28]. As shown in Figure 1(d), the measured SERS spectrum for the pure 4-MBA molecules adsorbed on the GNR surface exhibits two intense peaks at 1075 cm^{-1} and 1585 cm^{-1}, corresponding to the ring breathing/υ(C-S) (1075 cm^{-1}) and υ8a aromatic ring vibrations (1585cm^{-1}) of 4-MBA[29-31]. Moreover, we conducted an additional DFT simulation (see Figure S2) to understand the characteristic peak (1075 cm^{-1}) and the calculated peak is located at 1097 cm^{-1} which consistent with the referred ones as expected. The peaks observed at 1281 and 1705 cm^{-1} can be assigned respectively to the υ(C-OH) and υ(C=O) vibrations of the protonated carboxyl group[32], and that at 852 and 1423 cm^{-1} respectively to the deformation band $\delta(COO^-)$ and the symmetric stretching mode $\upsilon_s(COO^-)$ of the deprotonated carboxylate group[33-34], indicating that the carboxyl groups of the pure 4-MBA on the GNRs adopt either a protonated or deprotonated configuration. Upon the addition of Pb^{2+}, the Raman peaks associated with the aromatic ring vibrations exhibit no shift; however, the Raman peaks associated with the protonated carboxyl groups (υ(C-OH) and υ(C=O)) diminish and even vanish. Additionally, the Pb^{2+} ion induces the $\upsilon_s(COO^-)$ and $\delta(COO^-)$ modes to red shift to 1402 and 846 cm^{-1}, respectively, suggesting the formation of carboxyl-Pb^{2+} coordination complex. Additionally, these SERS signals are found to be highly reproducible, as evidenced by the 15 independent SERS spectra randomly collected from

the same Pb^{2+}/4-MBA system (see Figure S3), showing negligible variation in both peak position and signal intensity.

In order to have a more comprehensive conformation analysis on the carboxyl-Pb^{2+} coordination complex, we carried out SERS measurements under varied pH environment since the carboxyl group can adopt either a protonated or deprotonated configuration upon varying the pH value of, or adding metal ions to, the solution[35]. By comparing the SERS spectra of the 4-MBA/GNR system and pure 4-MBA in water in Figure 2(a), we find the frequency and intensity of the Raman peaks associated with the protonated carboxyl group are similar in both environments (1281 vs. 1289 cm^{-1} and 1705 vs. 1705 cm^{-1}); however, the symmetric stretching mode for the deprotonated carboxylate group (1423 cm^{-1}) becomes very weak for the 4-MBA in water. Instead, a broad shoulder appears in the SERS spectrum of the 4-MBA in water in the range of 1350-1430 cm^{-1}, indicating that most carboxyl groups of 4-MBA are protonated in aqueous environment. This information is important for the formation of carboxyl-Pb^{2+} coordination complex because most complexation processes occur in aqueous environments (i.e. in water).

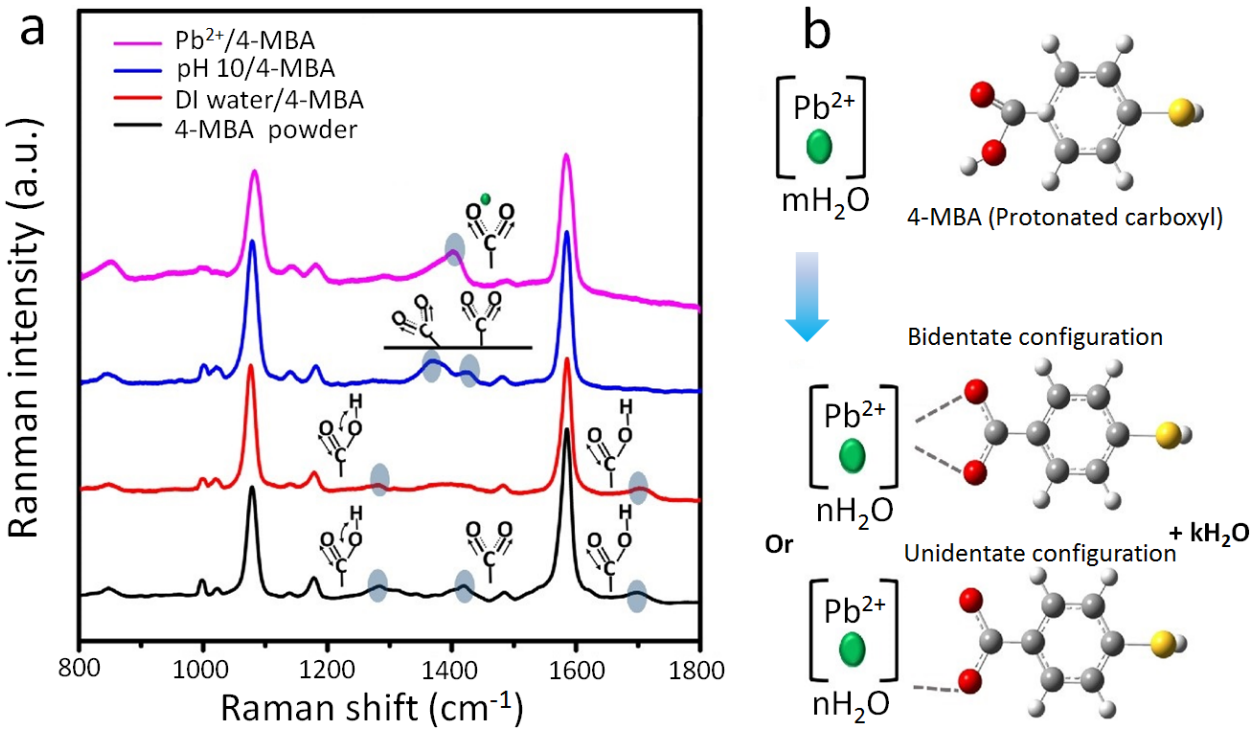

Figure 2. (a) SERS spectra of 4-MBA in different environments: adsorbed on GNRs (black), in DI water (red), in pH=10 alkaline environment (blue), and upon the addition of Pb^{2+} when adsorbed on the surface of GNRs (magenta). (b) Schematic illustration of two binding modes in the formation of carboxyl-Pb^{2+} coordination complex used in our DFT calculations. Here, a Pb^{2+}-aquo complex with mH_2O and a 4-MBA molecule with a protonated carboxyl group form a carboxylate-Pb^{2+} coordination complex having nH_2O and kH_2O (m = n + k).

Compared to the above-discussed Raman characteristics, the SERS spectrum for 4-MBA in the alkaline environment (pH = 10 in Figure 2(a)) exhibits dramatically different spectral features because the carboxyl group is very sensitive to the pH environment. Firstly, the two Raman peaks associated with the protonated carboxyl group (~1289 cm^{-1} and ~1705 cm^{-1}) disappear, indicating that all 4-MBA molecules are in the deprotonated carboxylate fashion. Secondly, two distinctive peaks emerge at 1363 and 1423 cm^{-1}, both of which can be ascribed respectively to a surface-bounded and an up-right symmetric stretching mode $\upsilon_s(COO^-)$ of the deprotonated carboxylate group, with their peak positions fully consistent with the previous report[36]. We can now conclude that the carboxyl group transforms from the protonated to deprotonated configuration with

increasing the pH value. Then, we turn to analyze the Pb^{2+}/4-MBA SERS spectrum in Figure 2(a) and observe no Raman peak associated with the protonated carboxyl group but a new peak at 1402 cm^{-1} corresponding to the υ_s(COO-Pb^{2+}) mode, which is different from that for the pure protonated carboxyl group (1363 or 1423 cm^{-1}). Therefore, we can now conclude that Pb^{2+} is coordinated to the carboxyl group by displacing a proton in the carboxyl group.

The above SERS spectral analysis provides a basic understanding on the conformational change of carboxyl-Pb^{2+} coordination complex. In fact, the carboxyl-Pb^{2+} binding configuration is jointly determined by the intrinsic cation property[37] and the metal-aquo complexation[38]. Typically, the carboxyl-metal coordination complexation can result in three binding configurations: unidentate, bidentate, and bridging[23]. To determine the exact carboxyl-Pb^{2+}coordination configuration, we resort to density function theory (DFT) calculations by modelling 4-MBA as a deprotonated carboxyl group due to the above discussion that Pb^{2+} replaces a bounded proton of the carboxyl group to form carboxyl-Pb^{2+} coordination complex. In the DFT modelling, the Pb^{2+} ion is placed either at the center of the two oxygen ions or at one side of the oxygen ion, as illustrated in Figure 2(b), forming either a bidentate and unidentate mode, respectively. By considering the Gibbs free energy of each species involved in the complexation process, we can achieve the most stable configuration for the carboxylate-hydrated Pb^{2+} coordination complex in which the final hydration number of Pb^{2+} is four and Pb^{2+} binds with the carboxylate group to form the most stable unidentate configuration (see detailed DFT calculation results in Figure S4). The unidentate coordination is a common configuration for carboxylate-metal complex in aqueous environment[37] as the hydrogen bond of the hydration molecule can stabilize the second oxygen of the carboxylate group[39-40]. Meanwhile, the Pb^{2+}-aquo solution is a kind of weak acid; thus, the charge acceptability of Pb^{2+} would not attract the second oxygen ion.

Based on the above SERS spectral analysis and the DFT calculation results, we can now propose that, in a carboxylate-Pb^{2+} coordination complex, the Pb^{2+} cation displaces the proton of, and binds to, the carboxyl group in a unidentate mode. To further verify this complexation process, we collected a series of Pb^{2+}/4-MBA SERS spectra under varied Pb^{2+} concentration. As shown in Figures 3(a), the carboxylate-Pb^{2+} vibrational mode, υ_s(COO-Pb^{2+}) at 1402 cm^{-1}, gradually diminishes with decreasing Pb^{2+} concentration, whereas the modes associated to the protonated carboxyl group at 1289 and 1705 cm^{-1} are restored. When the Pb^{2+} concentration is lowered to 1.25×10^{-7} M, the SERS spectrum of the coordination complex becomes similar to that of pristine 4-MBA in water. By normalizing the measured SERS spectra by the intensity at 1585 cm^{-1}, we plot relative intensity for the symmetric stretching peak related to carboxylate-Pb^{2+} (1402 cm^{-1}) and carboxyl vibration υ(C=O) (1705 cm^{-1}) in Figure S5(a) and (b) as a function of Pb^{2+} concentration. It can be seen that the normalized Raman intensity at 1402 cm^{-1} linearly decreases with the logarithm Pb^{2+} concentration, while that at 1705 cm^{-1} linearly increases. Besides the υ(C=O), an additional υ(C-COOH) peak[41] at ~800 cm^{-1} (see Figure S6) becomes increasingly significant with the decreasing Pb^{2+} concentration. Such opposite trends provide a complete picture of the carboxyl-Pb^{2+} complex formation, fully consistent with our proposed scenario that Pb^{2+} displaces the proton in the carboxyl group to form the ligand complex. Therefore, the SERS spectra of Pb^{2+}/4-MBA under low concentration Pb^{2+} tend to be similar with that of pristine 4-MBA in aqueous environment, i.e., restoring all features of the protonated carboxyl group.

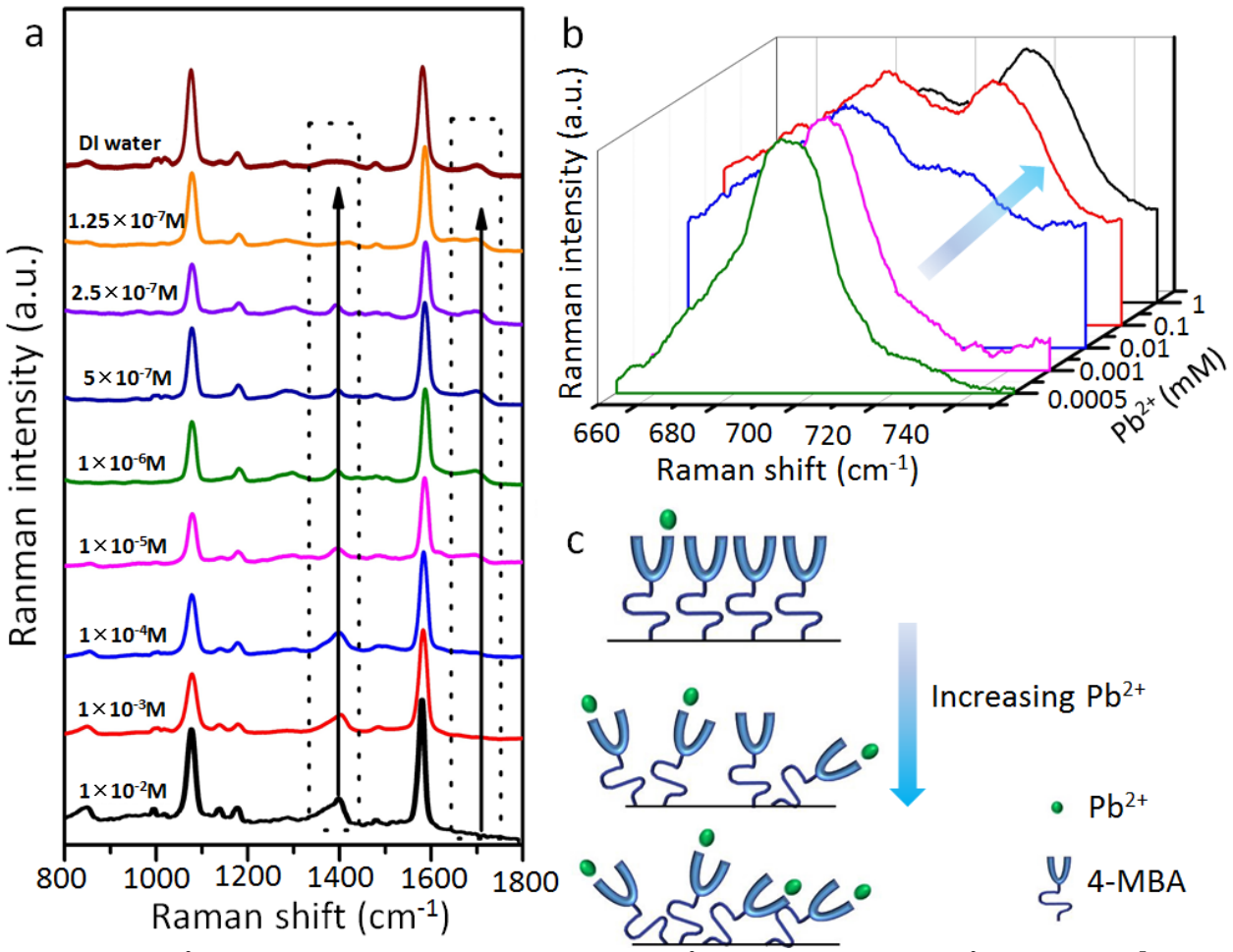

Figure 3. (a): Pb^{2+}-concentration-dependent SERS spectra of Pb^{2+}/4-MBA complex (1×10^{-2} M to 1.25×10^{-7} M) and pristine 4-MBA in DI water. (b) Magnified view of the same SERS spectra in the spectral range of 650 to 750 cm^{-1} as a function of Pb^{2+} concentration. (c) Schematic illustration of 4-MBA molecular orientation under varied Pb^{2+} concentration.

Interestingly, we also observe a weak Raman peak at 718 cm^{-1} in the magnified SERS spectra in Figure 3(b), the intensity of which also depends on Pb^{2+} concentration. With decreasing the Pb^{2+} concentration from 1 mM to 0.001 mM, this Raman peak intensity decreases dramatically and vanishes in the end. According to previous reports[35,40], this Raman mode could be ascribed to the out-of-plane vibration of υ(CCC), suggesting that the 4-MBA molecule in the complex possesses a tilted orientation with respect to the surface of gold as illustrated in Figure 3(c). It is worth to note that, the D.I water/4-MBA system shows no peak at 718 cm^{-1} (see Figure S7). Therefore, we

can conclude that under high concentration of Pb^{2+} ions, most carboxylate active sites are coordinated with Pb^{2+}, resulting in a high density of carboxyl-Pb^{2+} coordination complex. Subsequently, the repulsive interaction among these carboxylate-Pb^{2+} bonding leads to the down-tilted configuration of 4-MBA. When the Pb^{2+} concentration reaches a relatively low level, the peak at 718 cm^{-1} vanishes, suggesting that the repulsive interaction between adjacent 4-MBA molecules is insufficient and most of these molecules will remain upright configuration. In order to consider the electric neutralization effect from the anion solution, we conducted more DFT calculations to compare the binding energy between lead (II)-acetate and Pb^{2+}-4-MBA as a higher binding energy means the compounds more stable and has a stronger interaction. The calculated results in Figure S8 suggests that the binding energy of lead (II)-acetate is 1.722 eV while the value for Pb^{2+}-4-MBA is 2.716 eV. It is believed the hydrated Pb^{2+} would preferably bind to the 4-MBA carboxylate group with minimal effect on the free acetate (anion) in the solution. Therefore, at high Pb^{2+} concentrations, the 4-MBA molecules adopt a tilted orientation upon adsorption on the surface of the SERS substrate because of the repulsive interaction between adjacent carboxyl-ion complexes.

Since different carboxyl-ion coordination complexes have their unique SERS response, we can use such Raman spectral fingerprints to determine the identity of bound ions and their binding mode with 4-MBA. Here we select another five types of ions, including sodium (Na^+), potassium (K^+), calcium (Ca^{2+}), cerium (Ce^{3+}) and iron (Fe^{3+}). While the SERS spectra for the low-valence ions (Na^+, K^+, Ca^{2+}) share a similar vibration mode υ_s(COO-ion) at 1417 cm^{-1} and preserve the spectral features of the protonated carboxyl υ(C-OH) and υ(C=O) at 1281 and 1705 cm^{-1} (see Figure S9). These common features suggest that these ions (Na^+, K^+, Ca^{2+}) bind to the carboxyl group with a similar conformation, i.e. unidentate, protonated carboxyl. These SERS spectra

contrasts strikingly with that for the Pb^{2+} case, because the Raman peaks associated with the protonated carboxyl group vanish upon the addition of Pb^{2+}. However, the intensities of the two Raman modes at 1281 and 1705 cm^{-1} become significantly lower and even vanished for the Fe^{3+} and Ce^{2+} based complexes, indicating that the ions are bound to the active carboxylate active site by fully replacing the existing proton. It is noted that recently, M. Futamata and his co-workers performed some relevant work on SERS detection of different metal cations and p-MBA molecules.[42-43]

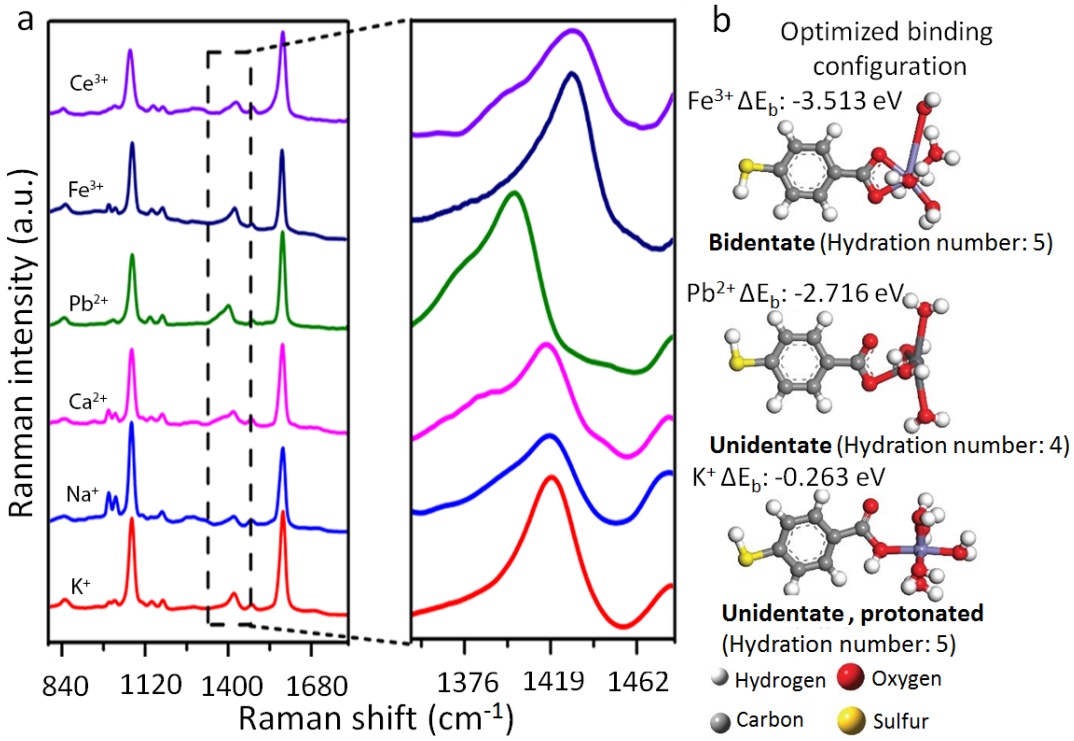

Figure 4. (a) SERS spectra of six carboxyl-ion coordination complex systems. The enlarged view in the spectral range from 1350 to 1485 cm^{-1} shows the symmetric stretching vibration $\upsilon_{s(COO\text{-ion})}$ of carboxyl. (b) DFT-calculated lowest-energy binding configurations for three carboxyl-ion complex systems. ΔE_b represents calculated binding energy for each complex.

To further confirm the above proposed mechanism, we calculated the lowest-energy binding configuration for two representative ions, K^+ and Fe^{3+}. The DFT results in Figure 4b render the

lowest energy binding configurations for K^+ (unidentate, protonated carboxyl), Pb^{2+} (unidentate, deprotonated carboxyl), and Fe^{3+} (bidentate, deprotonated carboxyl). This explains the preserved Raman features of the protonated carboxyl group in the SERS spectra. More importantly, the measured peak position of υ_s (COO-ion) of monovalent and divalent cations with lower wavenumbers, whereas the υ_s(COO-ion) frequency for trivalent cations with larger wavenumbers. In this case, we conducted DFT simulations to investigate the ligand interaction in carboxyl-metal-ion complex systems. The typical characteristic peak position of carboxylate symmetric vibration $\upsilon_s(COO^-)$ was selected for comparison since the low valence ions (such as Pb^{2+}) bind in a unidentate geometry whereas the high valence ions (such as Fe^{3+}) are bidentate. As shown in Figure S10 and Table S1, it is obvious that the $\upsilon_s(COO^-Fe^{3+})$ has a much higher wavenumber shift than that for $\upsilon_s(COO^-Pb^{2+})$, which is consistent well with our experimental results. This phenomenon can also be explained by the optimized binding configurations and pervious spectroscopic studies[44-45]. Generally, the frequency of υ_s(COO-ions) has a lower wavenumber in unidentate configuration and a higher wavenumber in bidentate configuration.

Finally, we also analyzed the binding energy (ΔEb) of three representative ions with the carboxyl group. Considering the calculated ΔEb of these three ions ($K^+ < Pb^{2+} < Fe^{3+}$), we can conclude that binding affinity is strongly correlated with ion valence. Trivalent and divalent ions have a higher charge acceptability, and thus the complex stability is larger than those monovalent cations. This also explains that Fe^{3+} has an optimized bidentate configuration, because trivalent ions have enough charge acceptability to attract charges from the second oxygen of carboxyl group[37].

In conclusion, we have systematically investigated the ligand interaction and conformation change in carboxyl-metal-ion complex systems through combining resonant SERS spectroscopy and DFT calculations. By comparing the Raman wavenumber shift between pristine carboxyl and

carboxyl-metal ion complexes (both adsorbed on a resonant solid SERS substrate), we have observed distinguishable conformation changes in the carboxyl-group molecule, 4-MBA. Additionally, at high Pb^{2+} concentrations, the 4-MBA molecules adopt a tilted orientation upon adsorption on the surface of the SERS substrate due to the repulsive interaction between adjacent carboxyl-ion complexes, which is manifested by the appearance of an out-of-plane vibration mode of the carboxyl group. Finally, we find that binding configuration of carboxyl-metal-ion complex depends on the valence of bound ions, and the observed general tendency is consistent with the DFT optimized lowest-energy configurations. This easy-to-implement resonant SERS approach provides a useful means to probe ligand interaction and detect heavy metal ions.

ASSOCIATED CONTENT

Supporting Information

The Supporting Information is available free of charge on the

ACS Publications website at DOI:xxxx

AUTHOR INFORMATION

#Willis Kwun Hei Ho, Zhi Yong Bao, Xiaorong Gan contribute equally to this work.

The authors declare no competing financial interests.

ACKNOWLEDGMENT

This work was supported by the Hong Kong Polytechnic University (Grant No. 1-ZVH9). The authors acknowledge the National Natural Science Foundation of China (Grant No. 51802066) and the Fundamental Research Funds for the Central Universities of China (Grant No. JZ2019YYPY0023).

REFERENCES

[1] Antonini, E.; M. Brunori. Hemoglobin and Myoglobin. Elsevier, Amsterdam, London, **1971**.

[2] Baldwin, J.; Chothia, C. Haemoglobin: the structural changes related to ligand binding and its allosteric mechanism. *J. Mol. Bio.* **1979**, 129, 175-220.

[3] Tuerk, C.; Gold, L. Systematic evolution of ligands by exponential enrichment: RNA ligands to bacteriophage T4 DNA polymerase. *Science* **1990**, 249, 505-510.

[4] Beese, L S.; Steitz, T. A. Structural basis for the 3'-5' exonuclease activity of Escherichia coli DNA polymerase I: a two metal ion mechanism. *EMBO J*. **1991**, 10, 25-33.

[5] Zheng, J.; Knighton, D. R.; Ten Eyck, L. F.; Karlsson, R.; Xuong, N. H.; Taylor, S. S.; Sowadski J. M. Crystal structure of the catalytic subunit of cAMP-dependent protein kinase complexed with magnesium-ATP and peptide inhibitor. *Biochemistry* **1993**, 32, 2154-2161.

[6] Pecoraro, V. L.; Hermes, J. D.; Cleland, W. W. S. Stability constants of magnesium and cadmium complexes of adenine nucleotides and thionucleotides and rate constants for formation and dissociation of magnesium-ATP and magnesium-ADP. *Biochemistry* **1984**, 23, 5262-5271.

[7] Younkin, T. R.; Connor, E. F.; Henderson, J. I.; Friedrich, S. K.; Grubbs, R. H.; Bansleben, D. A. Neutral, single-component nickel (II) polyolefin catalysts that tolerate heteroatoms. *Science* **2000**, 287, 460-462.

[8]. Herrmann, W.A.; Kohlpaintner, C.W.; Water-soluble ligands, metal complexes, and catalysts: Synergism of homogeneous and heterogeneous catalysis. *Angew. Chem. Int. Ed*. **1993**, 32, 1524-1544.

[9] Arashiba, K.; Miyake, Y.; Nishibayashi, Y. A. A molybdenum complex bearing PNP-type pincer ligands leads to the catalytic reduction of dinitrogen into ammonia. *Nat. Chem.* **2011**, 3, 120-125.

[10] Kaes, C.; Hosseini, M. W.; Rickard, C. E.; Skelton, B. W.; White, A. H. Synthesis and Structural Analysis of a Helical Coordination Polymer Formed by the Self-Assembly of a 2,2'-Bipyridine-Based exo-Ditopic Macrocyclic Ligand and Silver Cations. *Angew. Chem. Int. Ed*. **1998**, 37, 920-922.

[11] Kamiyama, A.; Noguchi, T.; Kajiwara, T.; Ito, T. Angew. A Graphite-Like Complex with Large Cavities Constructed with the Complex Ligand. *Chem. Int. Ed.* **2000**, 39, 3130-3132.

[12] Nienaber, V. L.; Richardson, P. L.; Klighofer, V.; Bouska, J. J.; Giranda, V. L.; Greer, J. Discovering novel ligands for macromolecules using X-ray crystallographic screening. *Nat. Biotechnol*. **2000**, 18, 1105-1108.

271. [13] Sherman, S. E.; Gibson, D.; Wang, A. H.; Lippard, S. J. X-ray structure of the major adduct of the anticancer drug cisplatin with DNA: cis-[Pt(NH3)2(d(pGpG))]. *Science* **1985**, 230, 412-417.
[15] Penner‐Hahn, J. E. X-ray absorption spectroscopy in coordination chemistry. *Coord. Chem. Rev*. **1999**, 190, 1101-1123.

[16] Kimber B.J.; Feeney J.; Roberts G.C.; Birdsall B.; Griffiths D.V.; Burgen A.S.; Sykes B.D. G.; Proximity of two tryptophan residues in dihydrofolate reductase determined by 19F NMR. *Nature* **1978**, 271, 184-5.

[17] Liao, J. H.; Dhayal, R. S.; Wang, X.; Kahlal, S.; Saillard, J. Y.; Liu, C. W. Neutron Diffraction Studies of a Four-Coordinated Hydride in Near Square-Planar Geometry. *Inorg. Chem*. **2014**, 53, 11140-11145.

[18] Liu, T.; Wang, X.; Hoffmann, C.; DuBois, D. L.;Bullock, R. M. Heterolytic cleavage of hydrogen by an iron hydrogenase model: an Fe-H···H-N dihydrogen bond characterized by neutron diffraction. *Angew. Chem. Int. Ed*. **2014**, 53, 5300-5304.

[19] Callender, R.; Deng, H. Nonresonance Raman difference spectroscopy: a general probe of protein structure, ligand binding, enzymatic catalysis, and the structures of other biomacromolecules. *Annu. Rev. Biophys. Biomol. Struct.* **1994**, 23, 215-245.

[20] Suzuki, H.; Taguchi, Y.; Sugiura, M.; Boussac, A.; Noguchi, T. Structural Perturbation of the Carboxylate Ligands to the Manganese Cluster upon Ca^{2+}/Sr^{2+} Exchange in the S-State Cycle of Photosynthetic Oxygen Evolution As Studied by Flash-Induced FTIR Difference Spectroscopy. *Biochemistry* **2006**, 45, 13454-13464.

[21] Carey, P. R.; Dong, J. Following Ligand Binding and Ligand Reactions in Proteins via Raman Crystallography. *Biochemistry* **2004**, 43, 8885-8893.

[22] Adnet, F.; Liquier, J.; Taillandier, E.; Singh, M. P.; Rao, K. E.; Lown, J. W. FTIR study of specific binding interactions between DNA minor groove binding ligands and polynucleotides. *J. Biomol. Struct. Dyn.* **1992**, 10, 565-575.

[23] Alvarez‐Puebla, R. A.; Liz‐Marzán, L. M. SERS detection of small inorganic molecules and ions. *Angew. Chem. Int. Ed.* **2012**, 51(45), 11214-11223.

[24] Kneipp, K.; Wang, Y.; Kneipp, H.; Perelman, L. T.; Itzkan, I.; Dasari, R. R.; Feld, M. S. Single Molecule Detection Using Surface-Enhanced Raman Scattering (SERS). *Phys. Rev. Lett.* **1997**, 78, 1667.

[25] McNay, G.; Eustace, D.; Smith, W. E.; Faulds, K.; Graham, D. Surface-enhanced Raman scattering (SERS) and surface-enhanced resonance Raman scattering (SERRS): a review of applications. *Appl. Spectrosc*.**2011**, 65, 825-837.

[26] Miller, M. M.; Lazarides, A. Sensitivity of Metal Nanoparticle Surface Plasmon Resonance to the Dielectric Environment. *J. Phys. Chem. B* **2005**, 109, 21556-21565.

[27] Chen, H.; Shao, L.; Li, Q.; Wang, J. Gold nanorods and their plasmonic properties. *Chem. Soc. Rev.* **2013**, 42, 2679-2724.

[28] Förstner, U.; Wittmann, G. T. Metal pollution in the aquatic environment. 2012 Springer Science & Business Media 2012.

[29] Park H, Lee SB, Kim K, Kim M. S. Surface-enhanced Raman scattering of p-aminobenzoic acid at silver electrode. *J. Phys. Chem*. **1990**, 94, 7576-7580.

[30] Honada, S.; Yu, Y. Y.; Futamata, M. Adsorbed state of p-mercaptobenzoic acid on silver nanoparticles. *Vib. Spectrosc.* **2014**, 128-133

[31] Li, R.; L, H.; Zhang, X.; Liu, P.; Chen, L.; Cheng. J.; Zhao. B.; Vibrational spectroscopy and density functional theory study of 4-mercaptobenzoic acid. *Spectrochim Acta A* **2015**, 148, 369-374.

[32] Lee, S. B.; Kim, K.; Kim, M. S. Surface-enhanced Raman scattering of p-mercaptobenzoic acid in silver sol. *J. Raman Spectrosc*. **1991**, 22, 811-817.

[33] Suh, J. S.; Kim J. Three distinct geometries of surface-adsorbed carboxylate groups. *J.Raman Spectrosc*.**1988**, 29, 143.

[34] Sun, F.; Hung, H. C.; Sinclair, A.; Zhang, P.; Bai, T.; Galvan, D. D; Yu, Q. Hierarchical zwitterionic modification of a SERS substrate enables real-time drug monitoring in blood plasma. *Nat. Commun.* **2016**, 7, 13437.

[35] Talley, C. E.; Jusinski, L.; Hollars, C. W.; Lane, S. M.; Huser, T. Intracellular pH sensors based on surface-enhanced raman scattering. Anal. Chem. **2004**, 76, 7064-7068.

[36] Michota, A.; Bukowska, J. Surface-enhanced Raman scattering (SERS) of 4-mercaptobenzoic acid on silver and gold substrates. *J. Raman Spectrosc*. **2003**, 34(1), 21-25.

[37] Ryde, U. Carboxylate binding modes in zinc proteins: A theoretical study. *Biophys. J* **1999**, 77(5), 2777-2787.

[38] Dudev, T.; Lim, C. Effect of Carboxylate-Binding Mode on Metal Binding/Selectivity and Function in Proteins. *Acc. Chem. Res.* **2007**, 40, 85-93.

[39] Dudev, T.; Lim, C. Monodentate versus Bidentate Carboxylate Binding in Magnesium and Calcium Proteins: What Are the Basic Principles? J. *Phys. Chem. B.* **2004**, 108, 4546-4557.

[40] Gómez, V.; Corbella, M. Versatility in the Coordination Modes of n-Chlorobenzoato Ligands: Synthesis, Structure and Magnetic Properties of Three Types of Polynuclear MnII Compounds. *Eur. J. Inorg. Chem*. **2009**, 4471-4482.

[41] Chaoxiong, M.; Joel M, Harris; Surface-Enhanced Raman Spectroscopy Investigation of the Potential-Dependent Acid−Base Chemistry of Silver-Immobilized 2-Mercaptobenzoic Acid. *Langmuir*. **2011**, 27, 3527-3533.

[42] Kuwana, R.; Handa, S.; Futamata, M.; Elucidation of hydrated metal ions using flocculation-surface enhanced Raman scattering. *Chem. Phys. Lett*. **2018**, 693, 79-83.

[43] Tabei, K.; Akai, K.; Futamata, M. Specific photocatalytic reaction of p-methyl thiophenol and related molecules under the gap mode resonance. *Chem. Phys. Lett*. **2019**, 730, 568-574.

[44] Deacon, G.B.; Phillips, R.J. Relationships between the carbon-oxygen stretching frequencies of carboxylato complexes and the type of carboxylate coordination. *Coord. Chem. Rev*. **1980**, 33, 227-250.

[45] Nara, M.; Torii, H.; Tasumi, M. Correlation between the Vibrational Frequencies of the Carboxylate Group and the Types of Its Coordination to a Metal Ion: An ab Initio Molecular Orbital Study. *J. Phys. Chem.* **1996**, 100, 19812-19817.

Supporting information

Experiment Section

1. Seed medicated growth of GNRs

The Au seed solution was prepared by adding Au (III) chloride trihydrate ($HAuCl_4$ 0.25 mL, 0.25 mM) into hexadecyltrimethylammonium bromide (CTAB 9.75 mL, 0.1 M) solution, followed by injecting ice-cold sodium borohydride ($NaBH_4$ 600 μL, 10 mM) to reduce the Au (III) ion into Au seeds. Then the seed solution was gently stirred for 1 min, the resultant mixture should be kept in room temperature at least 2 hours. The growth solution was prepared by adding $HAuCl_4$ (2 mL, 10 mM), sliver nitrate (0.4 mL, 400 μL), and ascorbic acid (320 μL, 0.1 M) into CTAB (5 mL, 0.20 M) solution with gentle mixing. Then the mixture color will change from yellowish to colorless. Finally, the prepared seed solution (80 μL) was added into the growth solution, and the resultant mixture was kept in room temperature overnight.

2. Deposition of GNRs on glass substrate

To prepare the resonant solid SERS substrate, the concentration of surfactant (CTAB) should be carefully controlled by centrifugation of prepared GNR for twice (5000 rpm, 15 mins) and then the treated GNRs were re-dispersed into deionized water. Meanwhile, the glass slide was cleaned by ultra-sonication in acetone, ethanol and deionized water for 30 min, respectively. Finally, the cleaned glass slide was immersed in the GNRs solution for 5 hours (the concentration of CTAB is estimated as 2.2 μM), a monolayer GNRs array would be assembled on the glass substrate.

3. Electron microscope characterization

The surface morphology of the resonant solid SERS substrate are characterized by scanning electron microscope (JEOL JSM-6335F) operating at 12 kV.

4. SERS measurements of 4-MBA and metal ions/4-MBA complex

The substrate is first soaked in the 5 mM 4-MBA ethanol solution and left it undistributed for 24 hours. Before the SERS measurements, the substrate is dried by nitrogen (N_2) gas. Then the SERS measurements are performed by using a Raman spectrometer from Princeton Instruments (HORIBA HR800) with an excitation laser wavelength of 633 nm. The laser power (with a beam diameter of 2 μm) was approximately 1 mW and the integration duration was kept constant at 1 s. The SERS measurement details for metal ions/4-MBA complex are similar to that for 4-MBA SERS sample.

Computational details.

All calculations for the binding processes between 4-MBA and metal ion hydration were performed using the DMol^3 code. The nonlocal GGA functional by Perdew and Wang (PW91) was used for all geometry optimizations. A basis set of numeric atomic functions (DNP) has been used after considering the water solvent effect. The binding energy (ΔE_b) between SERS molecule and metal ion hydration was calculated according to the following equation:

$$\Delta E_b = E(\text{SERS molecule} + M) - E(\text{SERS molecule}) - E(M)$$

where E(SERS molecule), E(M), and E(SERS molecule+M) represent the total energies of SERS molecule (4-MBA protonated/deprotonated), metal ion hydration, and their composite formed by the coordination interaction respectively.

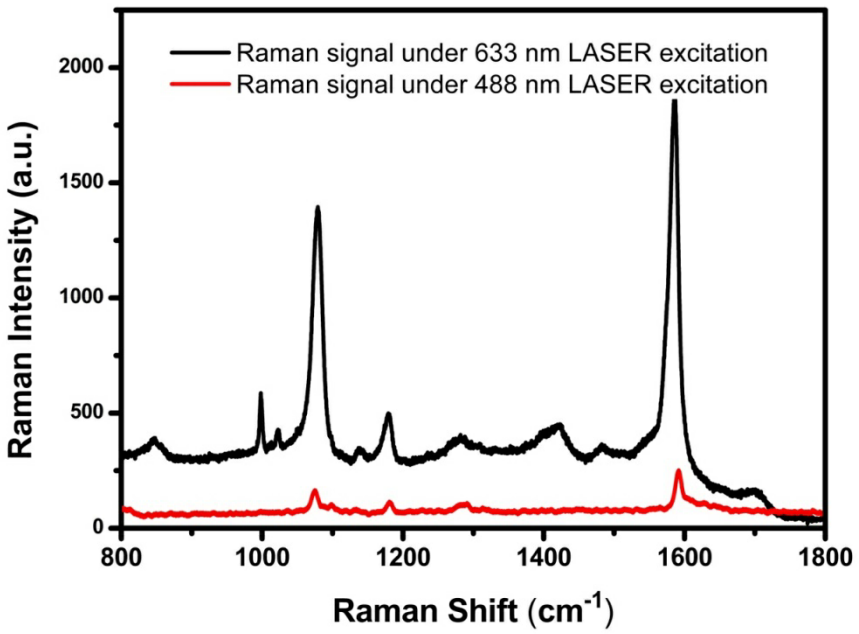

Figure S1. The SERS 4-MBA signal obtained from 633 nm laser excitations (black curve) and 488 nm (red curve).

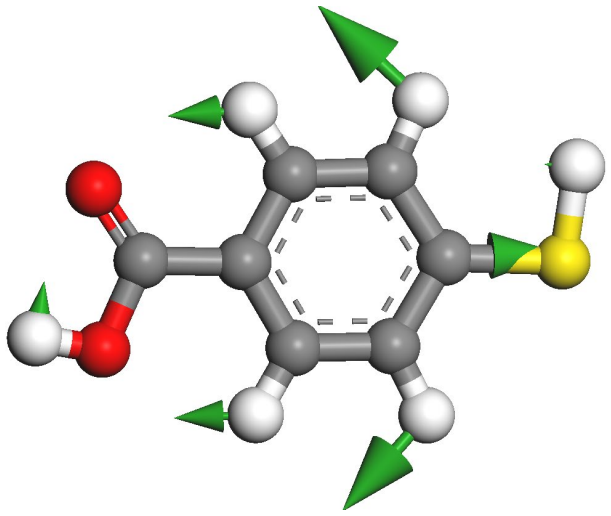

Figure S2. The calculated vibration mode at 1097 cm^{-1}, showing the breathing vibration of aromatic ring and υ(C-S). Green arrows indicate the atomic vibration direction.

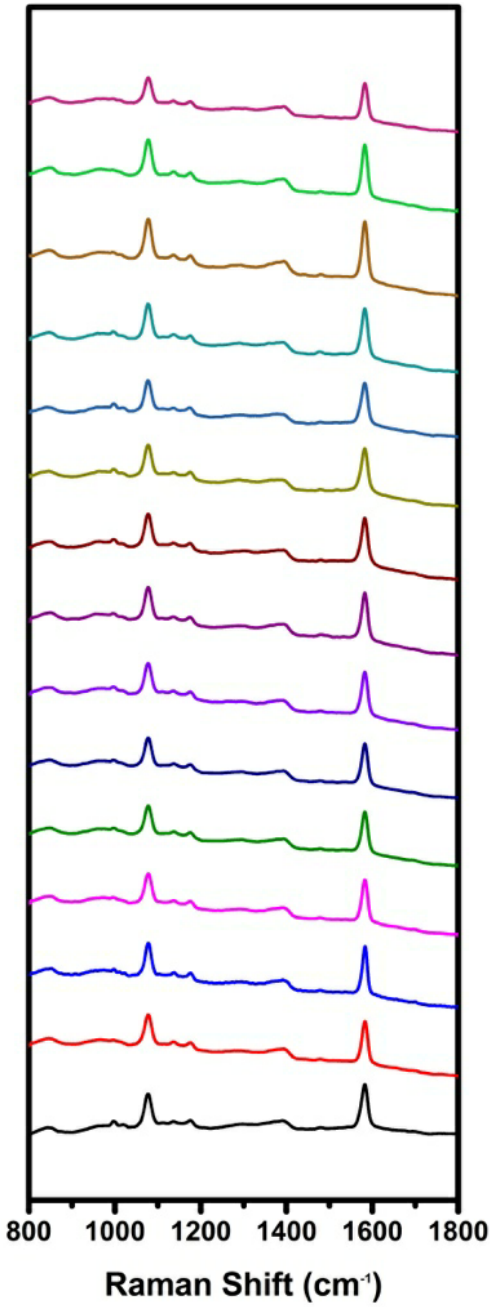

Figure S3. 15 independent SERS spectra for the Pb^{2+}/4-MBA system collected under resonant excitation at 633 nm.

Figure S4 DFT calculations on carboxylate-Pb^{2+} coordination complex

The most stable configuration is determined by the change of Gibbs free energy though the whole complexation which consider the free energy of each species. The most stable configuration of each case is highlighted in red color.

(a): Bidentate case

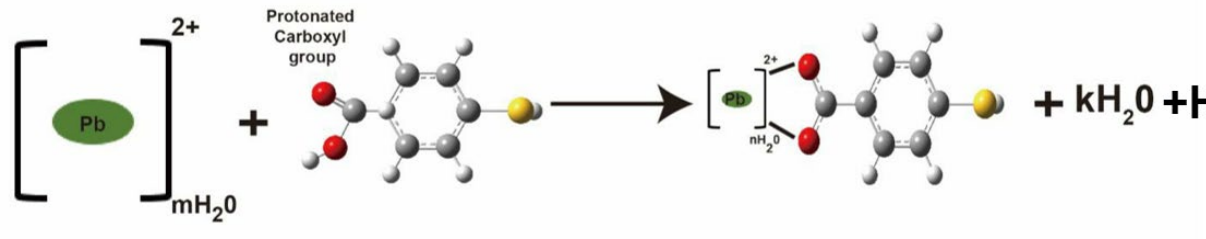

Free energy of Pb^{2+}- bidentate carboxylate complex (Ha)	Free energy of H_2O (Ha)	Free energy of Protonated carboxyl group (Ha)	Free energy of the most stable Pb^{2+} aqua complex $6H_2O$-Pb^{2+} (Ha)	ΔG (Ha)
(n=6)	(k=0)			
-20803.43124	0	-817.819	-19985.5332	-0.0790
(n=5)	(k=1)			
-20727.04397	-6.37596957	-817.819	-19985.5332	-0.0677
(n=4)	(k=2)			
-20650.65143	-152.752	-817.819	-19985.5332	-0.0512
(n=3)	(k=3)			
-20574.26304	-229.1279087	-817.819	-19985.5332	-0.0387
(n=2)	(k=4)			
-20497.86919	-305.5038783	-817.819	-19985.5332	-0.0208
(n=1)	(k=5)		6H2O-Pd2+	
-20421.46441	-381.8798479	-817.819	-19985.5332	0.0080

(b): Unidentate case

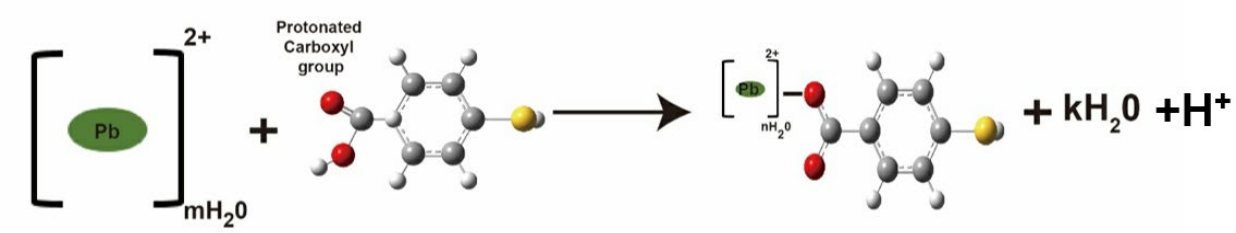

Free energy of Pb^{2+}-unidentate carboxylate complex (Ha)	Free energy of H_2O (Ha)	Free energy of Protonated carboxyl group (Ha)	Free energy of the most stable Pb^{2+} aqua complex $6H_2O$-Pb^{2+} (Ha)	ΔG (Ha)
(n=6)	(k=0)			
-20803.4	0	-817.819	-19985.5332	-0.0478
(n=5)	(k=1)			
-20727	-76.37596957	-817.819	-19985.5332	-0.0238
(n=4)	(k=2)			
-20650.7	-152.752	-817.819	-19985.5332	-0.0998
(n=3)	(k=3)			
-20574.3	-229.1279087	-817.819	-19985.5332	-0.0757
(n=2)	(k=4)			
-20497.9	-305.5038783	-817.819	-19985.5332	-0.0517
(n=1)	(k=5)		6H2O-Pb^{2+}	
-20421.5	-381.8798479	-817.819	-19985.5332	-0.0277

(c): Unidentate-protonated carboxyl case

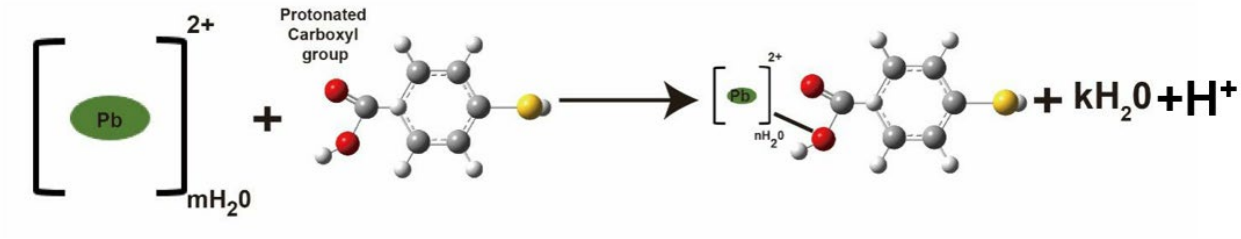

Free energy of Pb^{2+}-unidentate carboxylate complex (Ha)	Free energy of H_2O (Ha)	Free energy of Protonated carboxyl group (Ha)	Free energy of the most stable Pb^{2+} aqua complex $6H_2O$-Pb^{2+} (Ha)	ΔG (Ha)
(n=6)	(k=0)			
-20804.04262	0	-818.4660303	-19985.5332	-0.0434
(n=5)	(k=1)			
-20727	-76.37596957	-818.4660303	-19985.5332	-0.0342
(n=4)	(k=2)			
-20651.3	-152.752	-818.4660303	-19985.5332	-0.0140
(n=3)	(k=3)			
-20574.9	-229.1279087	-818.4660303	-19985.5332	0.0059
(n=2)	(k=4)			
-20498.5	-305.5038783	-818.4660303	-19985.5332	0.0280
(n=1)	(k=5)			
-20422.1	-381.8798479	-818.4660303	-19985.5332	0.0569

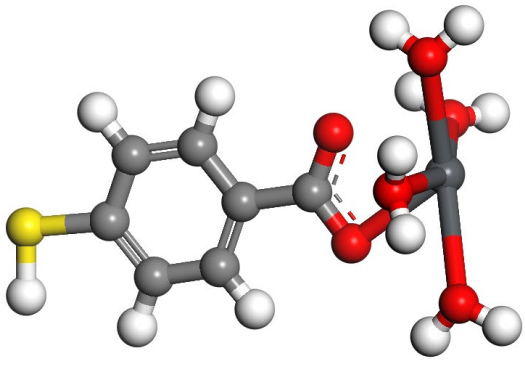

Having the change of Gibbs free energy of each case, the Unidentate-carboxylate case has found to be the most stable configuration (ΔG = -0.0998 Ha).

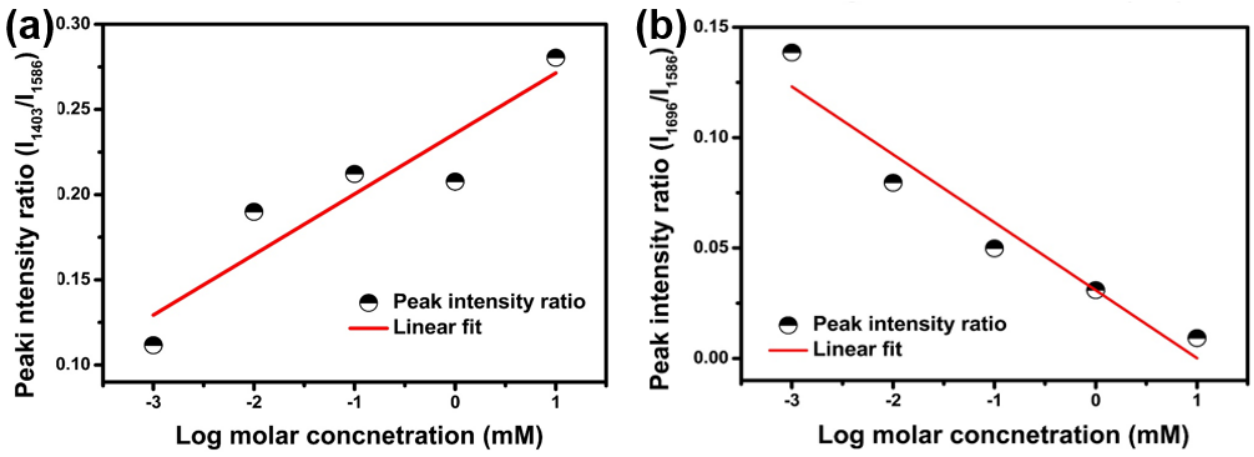

Figure S5. The relative peak intensity of peaks 1402 cm^{-1} (a) and 1696 cm^{-1} (b) vary with the Log molar Pb^{2+} concentration. The intensity is normalized to the maximum peak intensity at 1585 cm^{-1}.

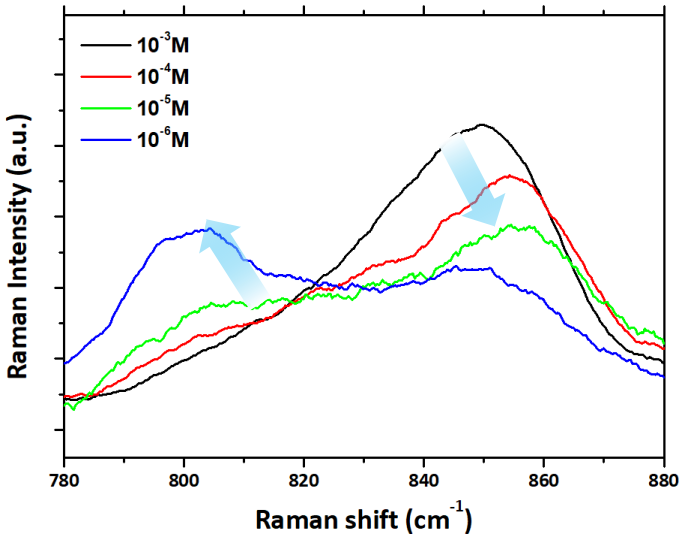

Figure S6. The 4-MBA SERS spectra with different Pb^{2+} concentration (10^{-3}M- 10^{-6}M). Note that, υ(C-COOH) is located at 800 cm^{-1}

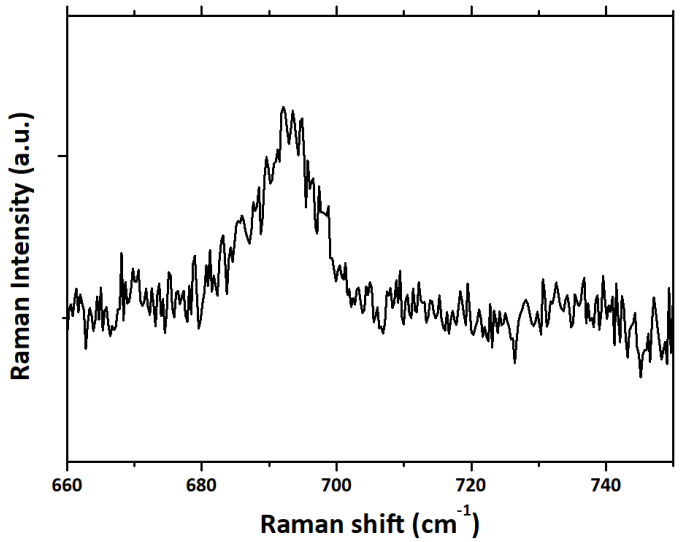

Figure S7. The 4-MBA SERS spectra of D.I. water/4-MBA system and no peak is found in 718 cm^{-1}.

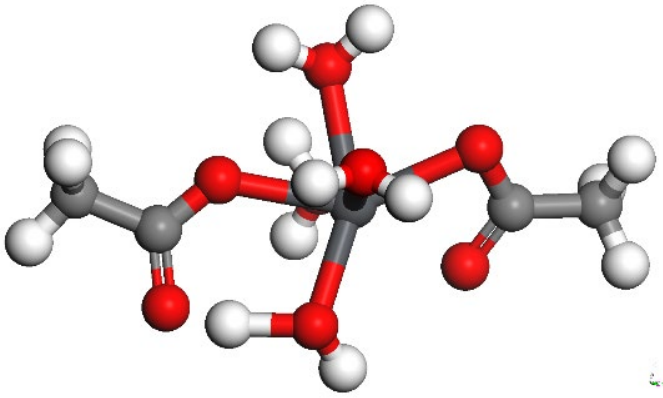

Figure S8. The calculated binding energy of lead (II)-acetate is 1.722 eV. The central Pb^{2+} ion coordinate to four H_2O and two acetates molecules.

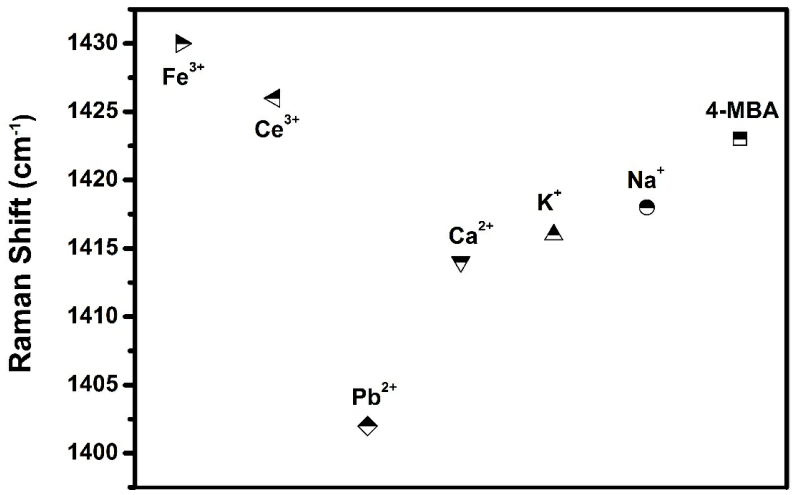

Figure S9. The peak position of υ_s (COO-metal ions) coordinated with different metal ions/4-MBA complex.

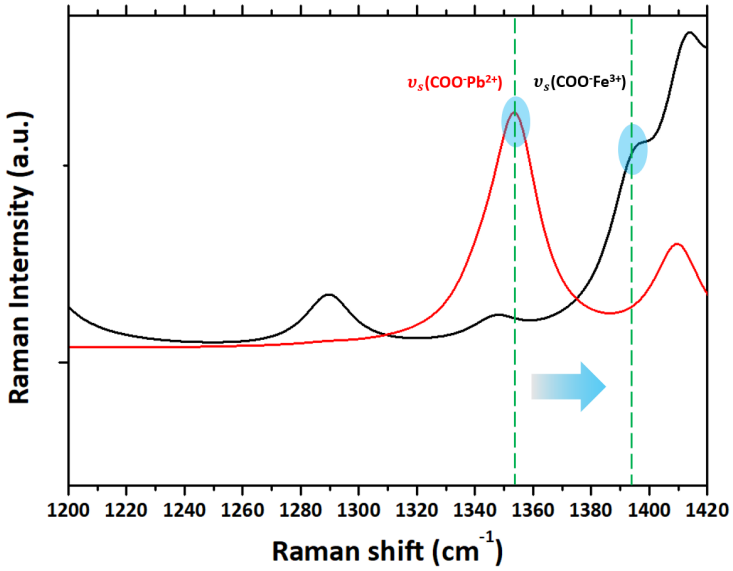

Figure S10. DFT calculated peak position of υ8a and υ_s(COO-M$^+$). The calculation is obtained by the optimized geometry of Pb^{2+}/4-MBA(Unidentate) and Fe^{3+}/4-MBA(Bidentate).

	υ8a	υ_s(COO-M$^+$)
Pb^{2+}/4-MBA	1554 cm^{-1} (1586 cm^{-1})	1353 cm^{-1} (1402 cm^{-1})
Fe^{3+}/4-MBA	1552cm^{-1} (1586 cm^{-1})	1395 cm^{-1} (1430 cm^{-1})

Table S1. DFT calculated Raman spectra of Pb^{2+}/4MBA and Fe^{3+}/4-MBA systems. The highlighted areas in blue indicate the peak position of υ_s(COO-ion).